Discovery of Open Cubane Core Structures for Biomimetic LnCo3 (OR)4 Water Oxidation Catalysts

Schilling, Mauro ; Hodel, Florian H ; Luber, Sandra

Abstract: Bio-mimetic catalysts such as LnCo3(OR)4 (Ln=Er, Tm; OR=alkoxide) cubanes have recently been in the focus of research for artificial water oxidation processes. Previously, the remarkable adaptability with respect to ligand shell, nuclear structure as well as protonation and oxidation states of those catalysts has been shown to be beneficial for the water oxidation process. We further explored the structural flexibility of those catalysts and present here a series of novel structures in which one metal center is pulled out of the cubane cage. This leads to an open cubane core, which is to some extent reminiscent of observed open/closed cubane-core forms of the oxygen-evolving complex in nature's photosystem II. We investigate how those open cubane core models alter the thermodynamics of the water oxidation cycle and how different solvation approaches influence their stability.

DOI: https://doi.org/10.1002/cssc.201701527

Supporting Information

The relative free energies ΔG_{i-0} were compared to the computational limit of water oxidation, i. e. the reaction free energy of water oxidation calculated with the same methods as the free energies of the catalytic state (108.2 kcal/mol for the CP2K calculations, and 115.5 kcal/mol for TURBOMOLE calculations using COSMO). The relative free energies were scaled by the ratio of the computational and experimental free energy of water oxidation, i.e. 113.5 kcal/mol / 108.2 kcal/mol = 1.05 (CP2K) and 113.5 kcal/mol / 115.5 kcal/mol = 0.98 (TURBOMOLE).

Thermodynamics – Different Solvation Models

Table S1. Relative free energies calculated for **{$ErCo_3(OR)_4$}** with explicit solvation shell; Free energy differences are given in kcal/mol.

State Si	ΔG_{Si-S0} (closed)	ΔG_{Si-S0} (open)	ΔG_{Si-S0} (closed) (no solvent)	ΔG_{Si-S0} (open) (no solvent)	$\Delta_{c-o}(\Delta G_{Si-S0})$ [a]	$\Delta_{c-o}(\Delta G_{Si-S0})$ (no solvent) [a]
S0	0.0	0.0	0.0	0.0	18.0	8.5
S1	37.7	36.1	19.9	23.3	19.6	5.3
S2	72.5	64.3	57.6	85.3	25.9	-18.3
S3	96.7	114.5	88.6	96.7	0.7	0.7
S4	120.5	138.9	117.3	131.4	0.2	-5.2

[a] including the zero-point corrected free energy difference between S0 (closed-open)

Table S2. Relative free energies calculated for **{$TmCo_3(OR)_4$}** with explicit solvation shell; Free energy differences are given in kcal/mol.

State Si	ΔG_{Si-S0} (closed)	ΔG_{Si-S0} (open)	ΔG_{Si-S0} (closed) (no solvent)	ΔG_{Si-S0} (open) (no solvent)	$\Delta_{c-o}(\Delta G_{Si-S0})$ [a]	$\Delta_{c-o}(\Delta G_{Si-S0})$ (no solvent) [a]
S0	0.0	0.0	0.0	0.0	6.3	12.2
S1	39.4	34.8	28.1	28.4	10.8	11.9
S2	61.1	53.6	30.4	77.9	15.5	-4.7
S3	117.8	103.5	84.9	121.7	20.1	-23.4
S4	144.8	122.3	110.2	130.8	28.1	-7.8

[a] including the zero-point corrected free energy difference between S0 (closed-open)

Table S3. Relative electronic energies calculated in TURBOMOLE between the catalyst structures optimized (opt) in TURBOMOLE using COSMO and without explicit solvent molecules the electronic energies of which were obtained from a single point calculation with Turbomole and COSMO (sp) on the catalyst structure of the geometry optimization including explicit solvation shell; Electronic energy differences are given in kcal/mol.

State Si	$\Delta E_{Si(opt)-Si(sp)}$ **{$ErCo_3(OR)_4$}** (closed)	$\Delta E_{Si(opt)-Si(sp)}$ **{$ErCo_3(OR)_4$}** (open)	$\Delta E_{Si(opt)-Si(sp)}$ **{$TmCo_3(OR)_4$}** (closed)	$\Delta E_{Si(opt)-Si(sp)}$ **{$TmCo_3(OR)_4$}** (open)
S0	-8.3	-7.8	-26.0	-20.2
S1	-10.4	-4.4	-31.5	-18.9
S2	-2.2	-13.9	-30.1	-11.8
S3	-15.3	-0.3	-22.7	-16.6
S4	-19.2	-1.3	-23.8	-12.0

Table S4. Relative free energies calculated for **{$ErCo_3(OR)_4$}** empolying either COSMO or DCOSMO-RS; Free energy differences are given in kcal/mol.

State Si	ΔG_{Si-S0} (COSMO) (closed)	ΔG_{Si-S0} (COSMO) (open)	ΔG_{Si-S0} (DCOSMO-RS) (closed)	ΔG_{Si-S0} (DCOSMO-RS) (open)
S0	0.0	0.0	0.0	0.0
S1	29.3	33.1	31.4	33.4
S2	69.6	65.2	72.1	55.6
S3	103.9	118.6	103.9	114.3
S4	121.8	137.5	120.6	134.8

Table S5. Relative free energies calculated for **{$TmCo_3(OR)_4$}** empolying either COSMO or DCOSMO-RS; Free energy differences are given in kcal/mol.

State Si	ΔG_{Si-S0} (COSMO) (closed)	ΔG_{Si-S0} (COSMO) (open)	ΔG_{Si-S0} (DCOSMO-RS) (closed)	ΔG_{Si-S0} (DCOSMO-RS) (open)
S0	0.0	0.0	0.0	0.0
S1	27.1	32.5	24.9	32.1
S2	62.5	80.8	56.6	68.6
S3	97.7	121.8	97.9	116.7
S4	119.7	136.1	115.6	132.7

Structure – Spin State

Table S6. Energetically prefered spin state (number of (a)lpha and number of (b)beta electrons) on active center (Co1) per catalytic intermediate including explicit solvation (using CP2K). Note: The other transition metal and lanthanide centers were assumed to maintain a high spin configuration. The spin states reported here correspond to the initial guess used for the calculations, the resulting spin state after the wavefunction optimization can vary.

states	**{$ErCo_3(OR)_4$}** (closed)	**{$ErCo_3(OR)_4$}** (open)	**{$TmCo_3(OR)_4$}** (closed)	**{$TmCo_3(OR)_4$}** (open)
S0	5a2b	5a2b	5a2b	5a2b
S1	5a1b	5a1b	4a2b	5a1b
S2	3a2b	3a2b	5a0b	3a2b
S3	3a3b	3a3b	5a1b	3a3b
S4	3a2b	3a2b	5a0b	3a2b

Table S7. Energetically prefered spin state (number of (a)lpha and number of (b)beta electrons) on active center (Co1) per catalytic intermediate using explicit solvation structures where the water molecules were deleted (CP2K). Note: The other transition metal and lanthanide centers were assumed to maintain a high spin configuration. The spin states reported here correspond to the initial guess used for the calculations, the resulting spin state after the wavefunction optimization can vary.

State Si	**{$ErCo_3(OR)_4$}**, (closed)	**{$ErCo_3(OR)_4$}** (open)	**{$TmCo_3(OR)_4$}** (closed)	**{$TmCo_3(OR)_4$}** (open)
S0	5a2b	5a2b	5a2b	5a2b
S1	5a1b	5a1b	4a2b	5a1b
S2	4a1b	5a0b	5a0b	4a1b
S3	5a1b	5a1b	5a1b	5a1b
S4	4a1b	5a0b	5a0b	5a0b

Table S8. Energetically prefered spin state (number of (a)lpha and number of (b)beta electrons) on active center (Co1) per catalytic intermediate using implicit solvation (TURBOMOLE). Note: The other transition metal and lanthanide centers were assumed to maintain a high spin configuration. The spin states reported here correspond to the initial guess used for the calculations, the resulting spin state after the wavefunction optimization can vary.

State Si	**{$ErCo_3(OR)_4$}** (closed)	**{$ErCo_3(OR)_4$}** (open)	**{$TmCo_3(OR)_4$}** (closed)	**{$TmCo_3(OR)_4$}** (open)
S0	5a2b	5a2b	5a2b	5a2b
S1	4a2b	5a1b	3a3b	5a1b
S2	4a1b	3a2b	4a1b	4a1b
S3	3a3b	5a1b	5a1b	5a1b
S4	3a2b	5a0b	4a1b	5a0b

Structure – Selected Bond Lengths

Table S9. Selected bond lengths of the open models of **{ErCo$_3$(OR)$_4$}** and **{TmCo$_3$(OR)$_4$}** (given in Å).

	{ErCo$_3$(OR)$_4$}			**{TmCo$_3$(OR)$_4$}**		
State Si – spin state	Co1-O1	Co1-O2	Co1-O3	Co1-O1	Co1-O2	Co1-O3
S0 – 5a0b	3.44	1.98	3.37	3.41	1.98	3.39
S1 – 3a3b	3.42	1.96	3.56	3.42	1.96	3.42
S1 – 4a2b	3.41	1.91	4.06	3.40	1.95	3.47
S1 – 5a1b	3.41	1.98	3.55	3.40	1.97	3.48
S2 – 3a2b	3.53	2.10	3.29	3.53	2.09	3.28
S2 – 4a1b	3.35	2.01	3.57	3.50	2.01	3.57
S2 – 5a0b	3.49	2.03	3.51	3.49	2.02	3.54
S3 – 3a3b	3.33	1.95	3.57	3.30	1.93	3.51
S3 – 4a2b	3.31	1.95	3.60	3.34	1.95	3.40
S3 – 5a1b	3.29	1.94	3.37	3.30	1.94	3.40
S4 – 3a2b	3.34	1.94	3.48	3.28	1.98	3.64
S4 – 4a1b	3.39	1.96	3.44	3.35	1.96	3.51
S4 – 5a0b	3.33	1.94	3.38	3.30	1.95	3.40

Table S10. Selected bond lengths of the closed models of **{ErCo$_3$(OR)$_4$}** and **{TmCo$_3$(OR)$_4$}** (given in Å).

	{ErCo$_3$(OR)$_4$}			**{TmCo$_3$(OR)$_4$}**		
state – spin state	Co1-O1	Co1-O2	Co1-O3	Co1-O1	Co1-O2	Co1-O3
S0 – 5a0b	2.15	2.13	2.19	2.13	2.13	2.19
S1 – 3a3b	2.12	2.06	2.08	2.12	2.07	2.08
S1 – 4a2b	2.01	1.97	2.06	2.00	1.99	2.25
S1 – 5a1b	2.17	2.16	2.17	2.17	2.18	2.17
S2 – 3a2b	2.13	2.06	2.02	2.15	2.05	2.07
S2 – 4a1b	20.6	2.01	2.21	2.05	2.02	2.23
S2 – 5a0b	2.38	2.17	2.16	2.36	2.19	2.17
S3 – 3a3b	2.0	1.97	1.98	2.07	2.02	2.13
S3 – 4a2b	1.98	1.98	2.22	1.98	1.99	2.23
S3 – 5a1b	2.11	2.09	2.19	2.10	2.09	2.21
S4 – 3a2b	2.04	2.00	1.98	2.17	2.05	2.02
S4 – 4a1b	2.04	2.03	2.21	2.03	2.03	2.23
S4 – 5a0b	2.14	2.21	2.18	2.1	2.1	2.20

Table S11. Shared electron numbers (SENs) for selected bonds within the cubane core of **{ErCo$_3$(OR)$_4$}** along the reaction path for the transition from the closed to the open structure.

SEN	closed	approx. transition state	open
$\sigma_{Co1\text{-}Co3}$	0.02	0.01	0.00
$\sigma_{Co1\text{-}Er}$	0.08	0.03	0.00
$\sigma_{Co1\text{-}O1}$	0.18	0.07	0.01
$\sigma_{Co1\text{-}O2}$	0.13	0.22	0.23
$\sigma_{Co1\text{-}O3}$	0.09	0.06	0.00

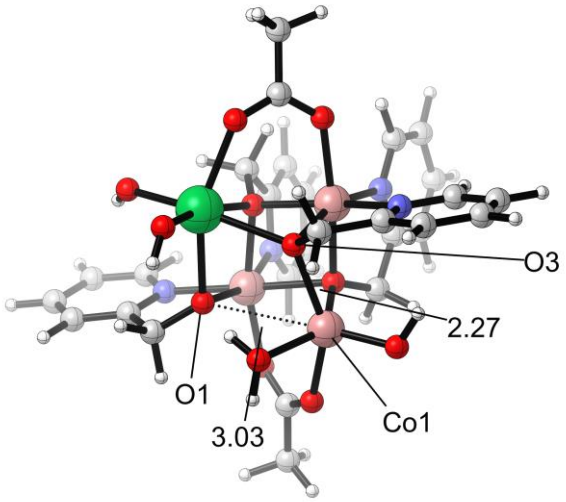

Figure S1. Transition state for the opening of **{TmCo$_3$(OR)$_4$}**, obtained by optimizing the maximum electronic energy structure from the approximate reaction pathway. The saddle point character of the transition state was verified by a vibrational analysis, which gave one imaginary frequency, a combination of a Co1-O1 and a Co1-O3 stretching vibration. The electronic activation barrier (B3LYP-D3/COSMO) $\Delta E_{el} = 3.9\ \mathrm{kcal/mol}$ is smaller than $\Delta E_{el} = 6.5\ \mathrm{kcal/mol}$ obtained for the approximate transition state, thus supporting the conclusion that the barrier for the opening of the catalytic ground state is reasonably small.

Thermodynamics – Mixed Open/Closed Reaction Pathway

Table S12. Mixed open/closed reaction pathways for **{ErCo$_3$(OR)$_4$**, the motifs are labeled as **c**(losed) or **o**(pen); Free energy differences are given in kcal/mol.

State Si	ΔG_{S0-Si} (CCCCC)	ΔG_{S0-Si} (**OO**CCC)	ΔG_{S0-Si} (**OOO**CC)	ΔG_{S0-Si} (C**OO**CC)	ΔG_{S0-Si} (CC**O**CC)	ΔG_{S0-Si} (**O**C**O**CC)	ΔG_{S0-Si} (**O**CCCC)
S0	0.0	0.0	0.0	0.0	0.0	0.0	0.0
S1	29.6	33.5	33.5	32.9	29.6	30.2	37.5
S2	77.1	70.9	65.9	65.4	65.4	65.9	78.2
S3	105.0	105.6	105.6	105.0	105.0	105.6	112.8
S4	123.1	123.6	123.6	123.1	123.1	123.6	130.9

Table S13. Mixed open/closed reaction pathways for **{TmCo$_3$(OR)$_4$}**, the motifs are labeled as **c**(losed) or **o**(pen); Free energy differences are given in kcal/mol,

states	ΔG_{S0-Si} (CCCCC)	ΔG_{S0-Si} (C**OO**CCC)	ΔG_{S0-Si} (**OOO**CC)	ΔG_{S0-Si} (**OO**CCC)	ΔG_{S0-Si} (**O**CCCC)	ΔG_{S0-Si} (CC**O**CC)	ΔG_{S0-Si} (**O**C**O**CC)
S0	0.0	0.0	0.0	0.0	0.0	0.0	0.0
S1	27.4	28.1	23.8	32.8	32.2	23.3	32.2
S2	63.2	76.9	81.6	67.9	67.9	76.9	81.6
S3	98.7	98.7	103.5	103.5	103.5	98.7	103.5
S4	121	121.0	125.7	125.7	125.7	121.0	125.7

Structures – Open and Closed Cage Structures

S0

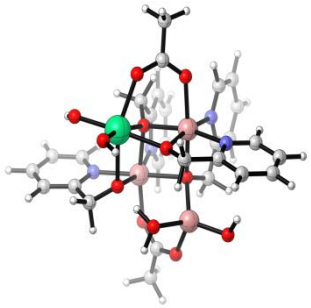

S1

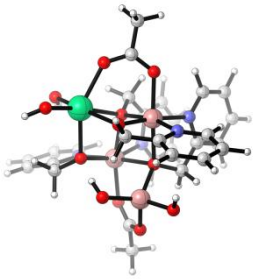

S2

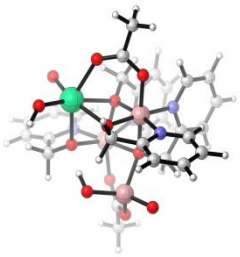

S3

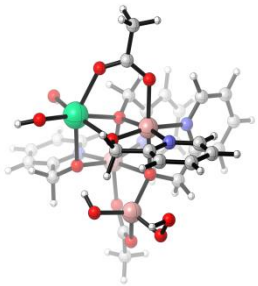

S4

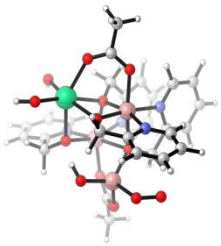

Figure S2. Open model of **{ErCo$_3$(OR)$_4$}** optimized with TURBOMOLE using the implicit solvent continuum model COSMO.

S0

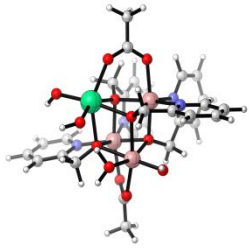

S1

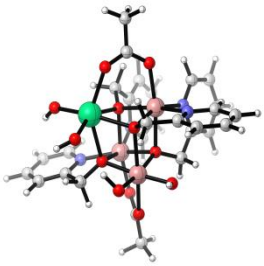

S2

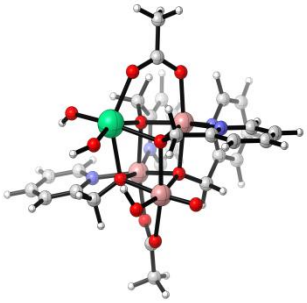

S3

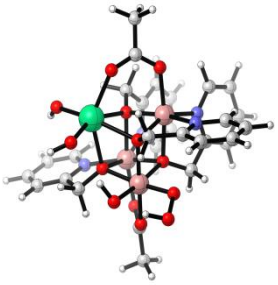

S4

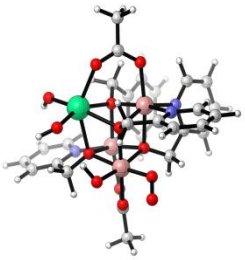

Figure S3. Closed model of **{$ErCo_3(OR)_4$}** optimized with TURBOMOLE using the implicit solvent model COSMO.

Frontier Orbitals – Intermediate S2

HOMO(a) HOMO(b)

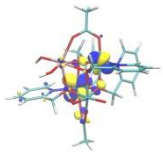

LUMO(a) LUMO(b)

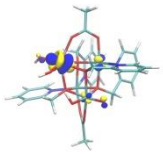

LUMO+1(a) LUMO+1(b)

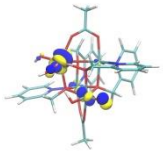

LUMO+2(a) LUMO+2(b)

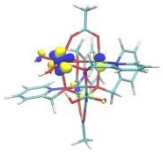

LUMO+3(a) LUMO+3(b)

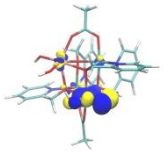

LUMO+4(a) LUMO+4(b)

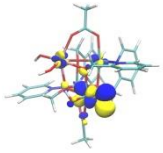

Figure S4. Canonical molecular orbitals of the closed structure of **{ErCo$_3$(OR)$_4$}** in the S2 state optimized with TURBOMOLE using the implicit solvent continuum model COSMO (isosurface 0.035 a.u. (blue), -0.035 a.u. (yellow)). The left column represents the alpha channel (a) and the right the beta channel (b) of the unrestricted Kohn-Sham DFT calculations.

HOMO(a)

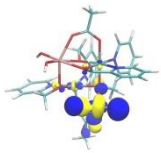

HOMO(b)

LUMO(a)

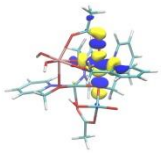

LUMO(b)

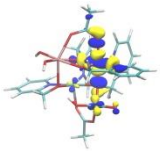

LUMO+1(a)

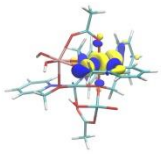

LUMO+1(b)

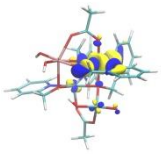

LUMO+2(a)

LUMO+2(b)

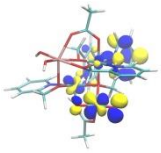

LUMO+3(a)

LUMO+3(b)

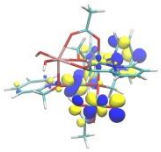

Figure S5. Canonical molecular orbitals of the open model of **{ErCo$_3$(OR)$_4$}** in the S2 state optimized with TURBOMOLE using the implicit solvent continuum model COSMO (isosurface 0.035 a.u. (blue), -0.035 a.u. (yellow)). The left column represents the alpha channel (a) and the right the beta channel (b) of the unrestricted Kohn-Sham DFT calculations.

HOMO(a) HOMO(b)

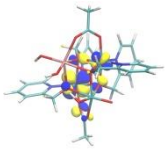

LUMO(a) LUMO(b)

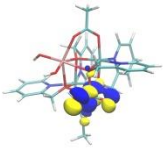

LUMO+1(a) LUMO+1(b)

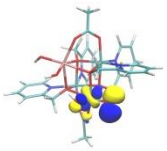

LUMO+2(a) LUMO+2(b)

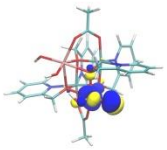

LUMO+3(a) LUMO+3(b)

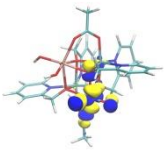

Figure S6. Canonical molecular orbitals of the closed model of **{TmCo$_3$(OR)$_4$}** in the S2 state optimized with TURBOMOLE using the implicit solvent continuum model COSMO (isosurface 0.035 a.u. (blue), -0.035 a.u. (yellow)). The left column represents the alpha channel (a) and the right the beta channel (b) of the unrestricted Kohn-Sham DFT calculations.

HOMO(a) HOMO(b)

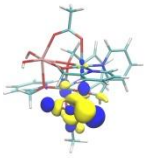

LUMO(a) LUMO(b)

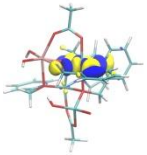

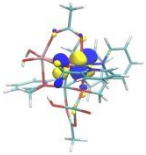

LUMO+1(a) LUMO+1(b)

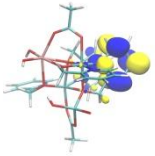

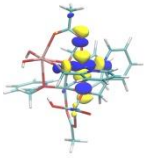

LUMO+2(a) LUMO+2(b)

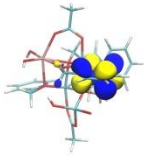

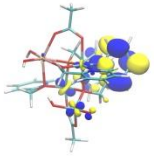

LUMO+3(a) LUMO+3(b)

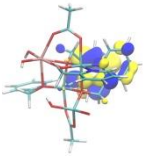

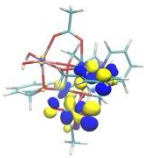

LUMO+4(a) LUMO+4(b)

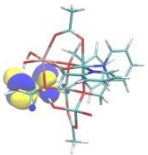

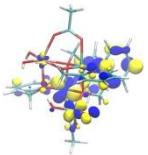

Figure S7. Canonical molecular orbitals of the open structure of **{$TmCo_3(OR)_4$}** in the S2 state optimized with TURBOMOLE using the implicit solvent continuum model COSMO (isosurface 0.035 a.u. (blue), -0.035 a.u. (yellow)). The left column represents the alpha channel (a) and the right the beta channel (b) of the unrestricted Kohn-Sham DFT calculations.

Structural Analysis of the Models with Explicit Solvation

We compared the open cage structures obtained with the lowest electronic energy multiplicities of each state of **{ErCo$_3$(OR)$_4$}** and **{TmCo$_3$(OR)$_4$}**: The structures of the S0 states do not show any significant differences. In S1 and S2, on the other hand, the Co1-O1 and Co1-O3 distances are 0.15 Å smaller in **{TmCo$_3$(OR)$_4$}** than in **{ErCo$_3$(OR)$_4$}** (see Figure S8). Furthermore, in both states, one OH ligand on Ln is oriented differently, depending on the nature of the lanthanide, leading also to a difference in the position of the hmp ligand next to it and the local water shell structure.

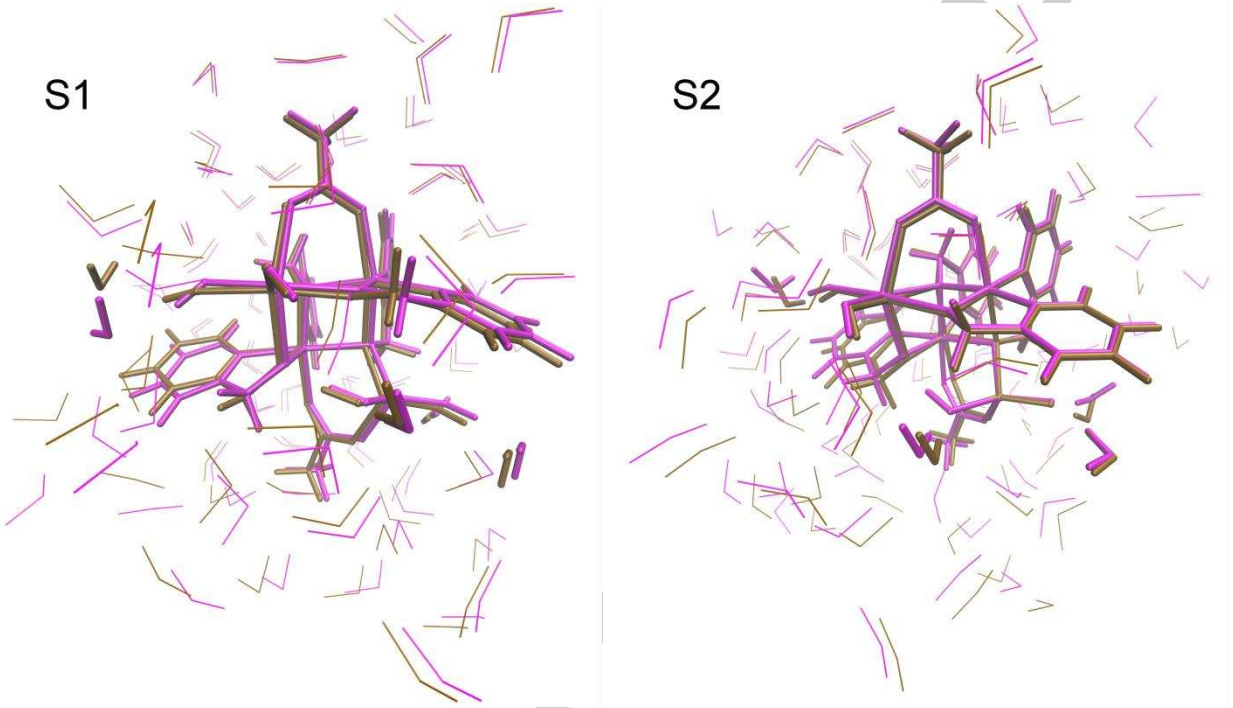

Figure S8. Comparison of the open structures of **{ErCo$_3$(OR)$_4$}** (magenta) and **{TmCo$_3$(OR)$_4$}** (ochre) in S1 and S2.

There are some differences in the structure of the cubane cage in S3 and S4 as well (the Co1-O3 in **{TmCo$_3$(OR)$_4$}** distance is 0.3 Å longer than the one in **{ErCo$_3$(OR)$_4$}**), but the orientation of the ligands and the structures of the solvent shells are similar. We were unable to discover any connection between the greater tendency of the closed cubane cage of **{TmCo$_3$(OR)$_4$}** compared to the one of **{ErCo$_3$(OR)$_4$}** to distort and the structural differences between the catalysts in their open cage structure.
To further study the influence of the lanthanide cation on the structure of the catalysts, we substituted Er in the closed cage structure of S2 and Tm in the closed and open cage structures of S2 with high-spin Co(III) and re-optimized the geometry. The distortions of the closed cubane cages remained, and also the open cage structure was found to be stable. We did not investigate other catalytic states, barriers, or whether those structures are lower or higher in energy than a potential undistorted {$Co^{II}_3Co^{III}$}-cubane. These calculations show, however, that while the degree of opening and the distortion of the cubane cages are dependent on the nature of the Ln^{3+} (or Co^{3+}) cation, the flexibility of the cage is not due to the lanthanide per se, but either hinges on the presence of a (3+)-cation at that position, or the ligand environment of **{ErCo$_3$(OR)$_4$}** and **{TmCo$_3$(OR)$_4$}**. Indeed, one can imagine that the exchange of a monodentate acetate ligand for hydroxide, which had been found to be thermodynamically favorable for **{ErCo$_3$(OR)$_4$}** and **{TmCo$_3$(OR)$_4$}**, might lend flexibility to the cubane cage.

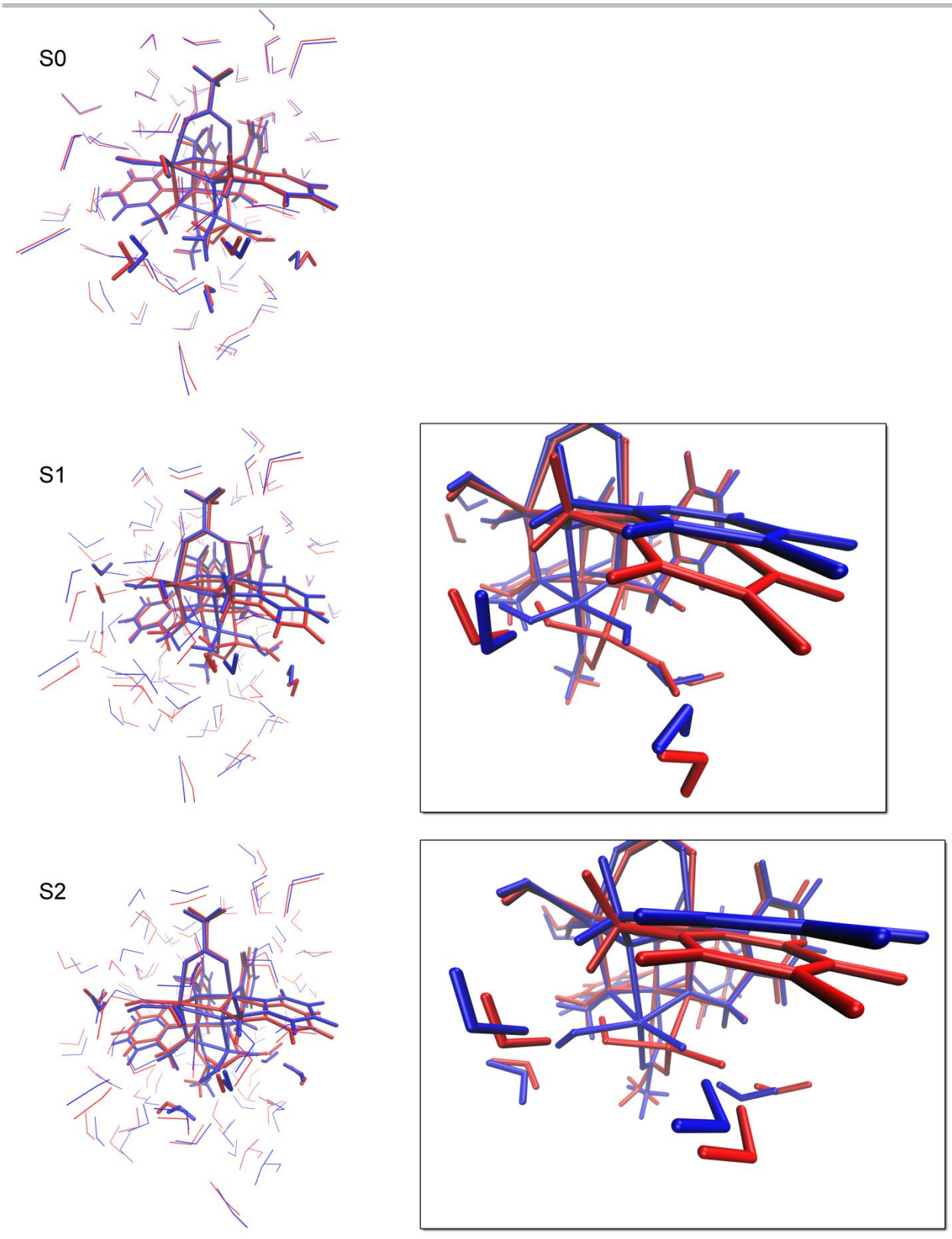

Figure S9. (Continued on the next page) Opened (red) and closed (blue) structures of **{ErCo$_3$(OR)$_4$}**.

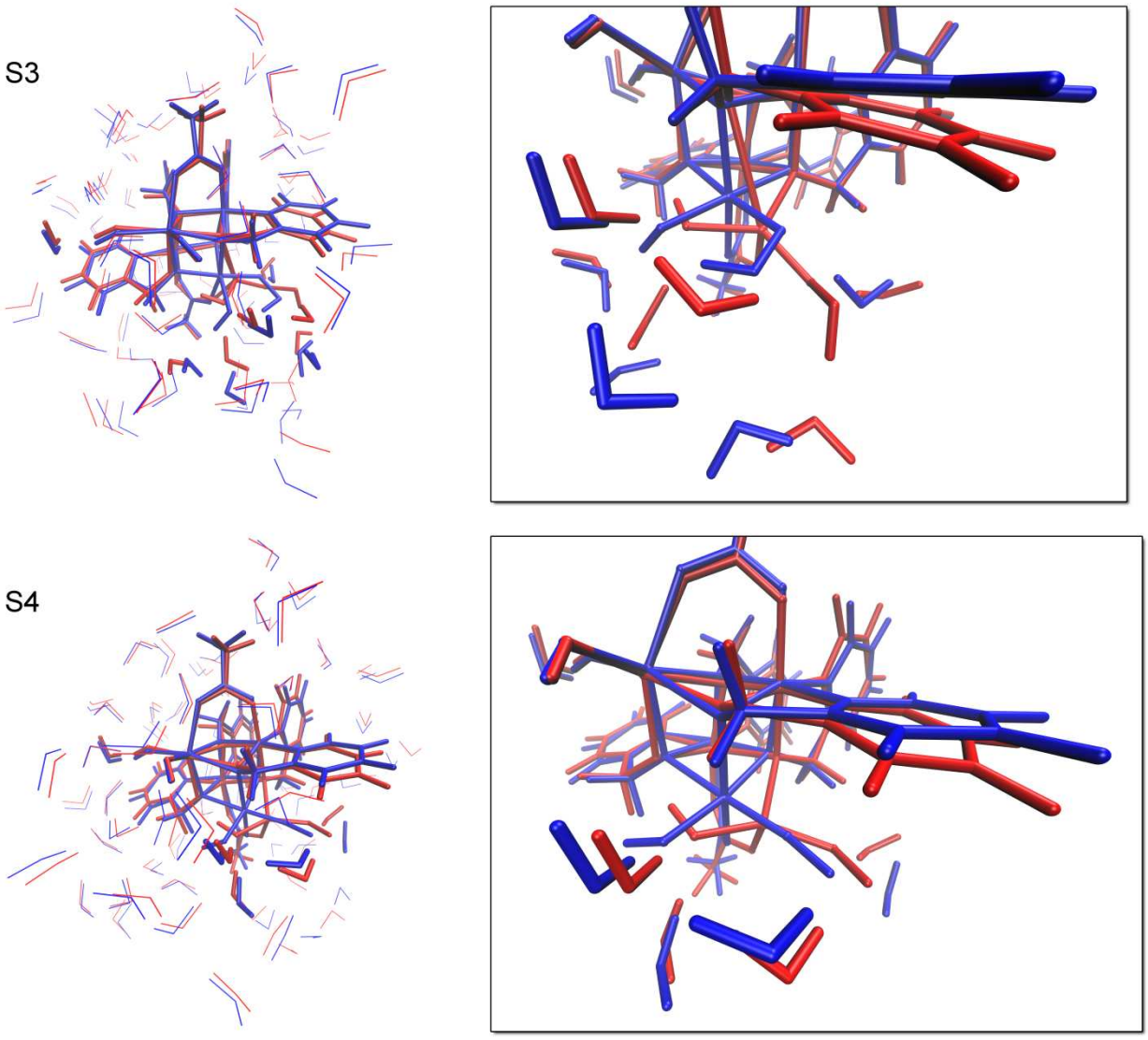

Figure S9. (Continued) Opened (red) and closed (blue) structures of **{ErCo$_3$(OR)$_4$}**.

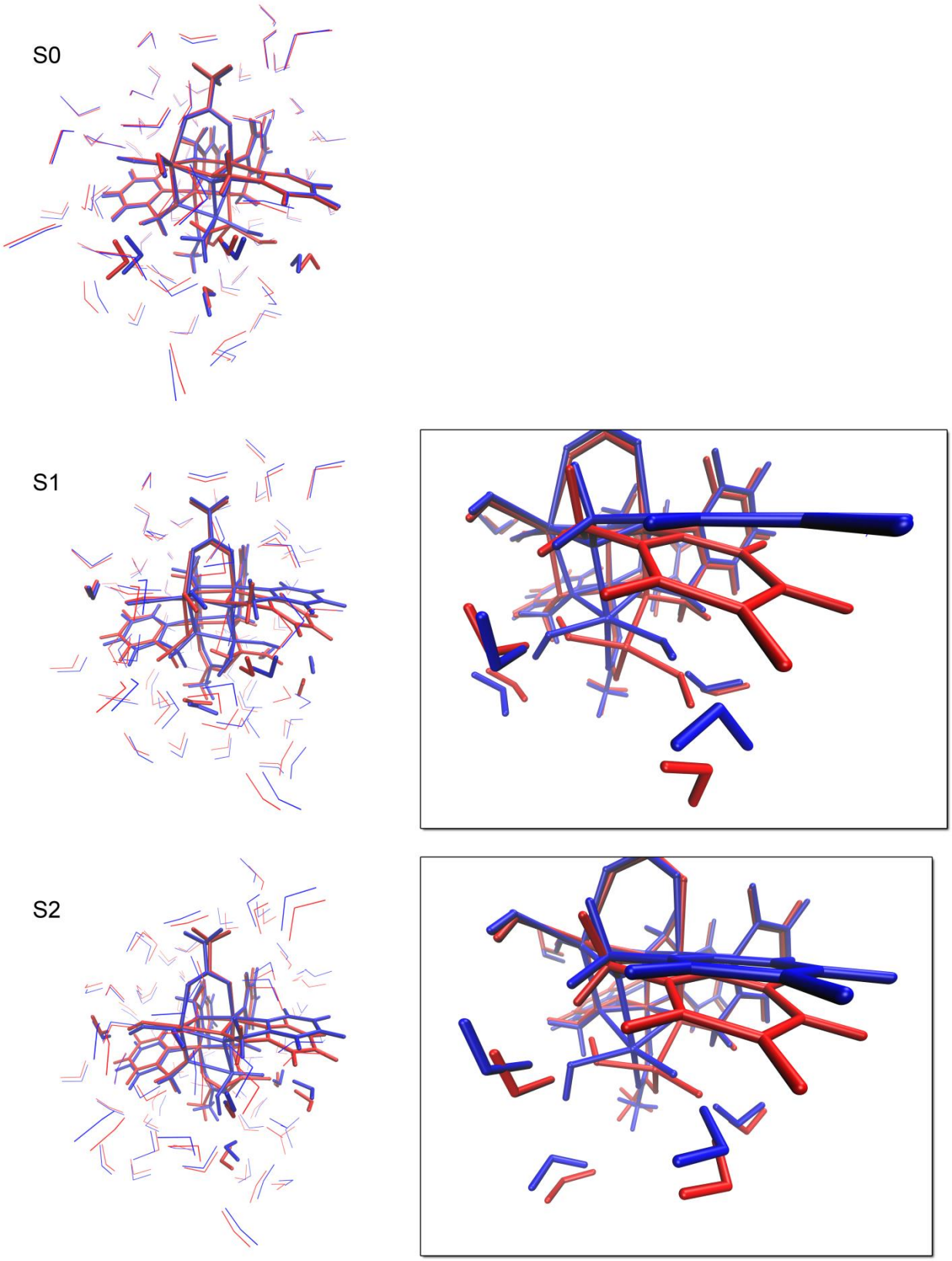

Figure S10. (Continued on the next page) Opened (red) and closed (blue) structures of **{TmCo$_3$(OR)$_4$}**.

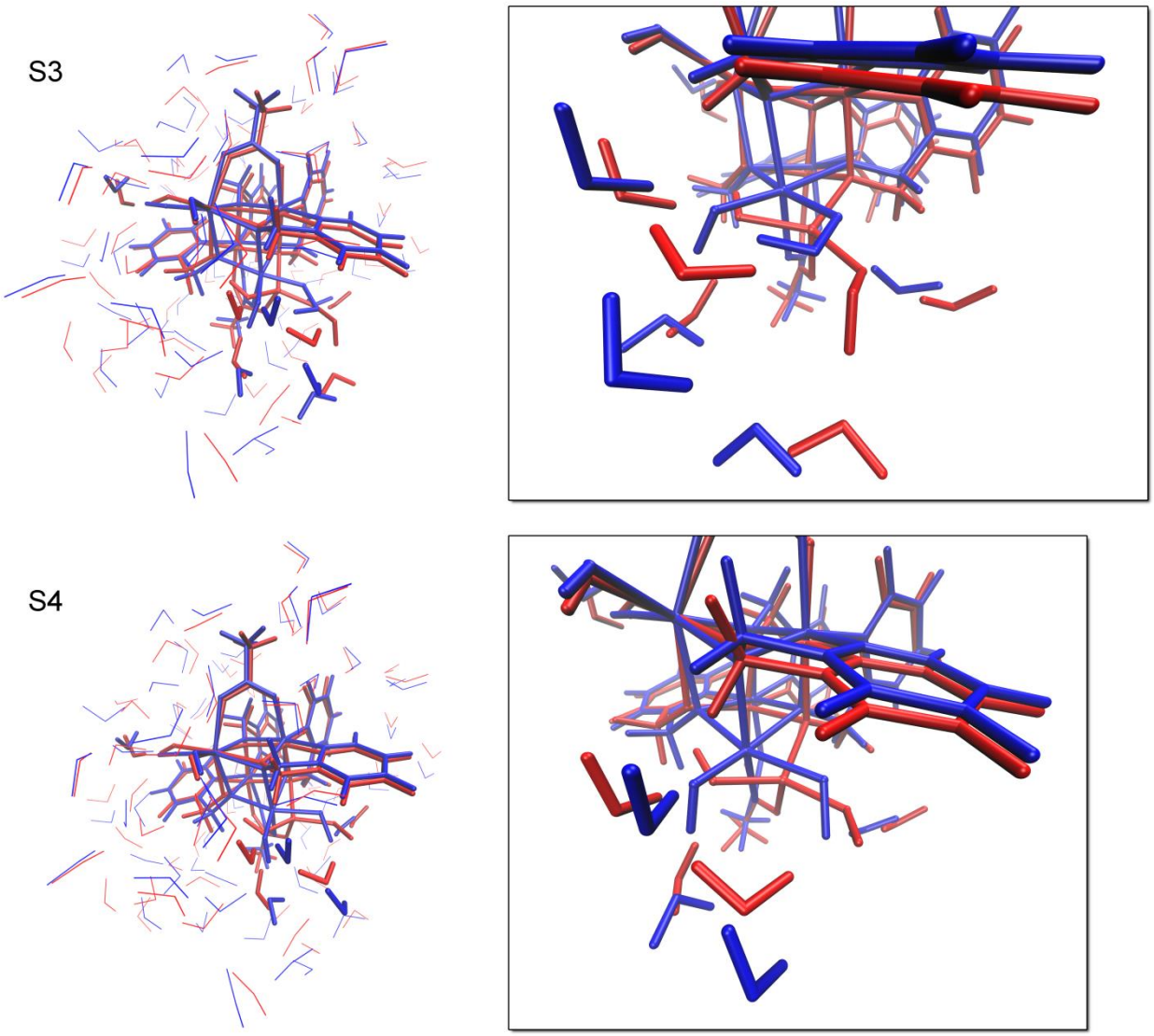

Figure S10. (Continued) Opened (red) and closed (blue) structures of **{TmCo$_3$(OR)$_4$}**

The prominent structural differences between the open and closed cage structures of the two catalysts are of course the Co1-O1 and Co1-O3 distances, which are 0.7-1.5 Å longer in the open cage structures, whereas the Co1-O2 distances are smaller (up to 0.2 Å). Apart from the water ligands of the S0 states, which are drawn 0.1 Å closer to Co1 by opening the cubane cage, the metal to ligand distances are unchanged. Their orientations vary however, as exemplified in Figures S9 and S10.

The differences between open and closed cage structures are smallest in S0 of both catalysts. The positions of the hmp ligands, the ligands, as well as the structures of the solvent shells are similar, except for the water and hydroxide ligands on Co1 and the water molecules directly hydrogen bonding to them.

In the subsequent states, the "inactive ligand" is not H_2O, which is donating 2 hydrogen bonds to solvent water and accepting one in the closed cage structure of S0, but hydroxide. In the closed cage structures of S1 and S2, this hydroxide ligand is accepting and donating one hydrogen bond, the donated one being broken during the cage opening. An exception to this is the closed cage structure of S1 of **{ErCo$_3$(OR)$_4$}**, in which the orientation of the hydroxide ligand is different from S1 of **{TmCo$_3$(OR)$_4$}** and the S2 states of both catalysts. It interacts with a different solvent water molecule and the distance between them is much longer than for the donating hydrogen bond of the other three systems (2.8 Å compared to 1.9 Å). This difference in ligand orientation is connected to the distortion of the cubane cage, which we had observed for the closed cage structures of S1 and S2 of **{TmCo$_3$(OR)$_4$}**, but only for S2 of **{ErCo$_3$(OR)$_4$}**.[1] In the open cage structure, the orientation of the "opening hydroxide" (ligand a) is very similar in all states.

Furthermore, the difference in the positions of one of the Ln-OH ligands and the water molecules interacting with it between the open and closed cage structure of S1 of **{ErCo$_3$(OR)$_4$}** is much larger than the one of S1 of **{TmCo$_3$(OR)$_4$}** or the S2 state of both catalysts. This ligand has not only a different orientation depending on the nature of the lanthanide in the open cage structure of S1 (see Figure S8), but also in the closed one.

The position of the hmp ligand on Co3 and O3 is changed by the opening of the cubane cage in the S1 and S2 states of **{ErCo$_3$(OR)$_4$}** and **{TmCo$_3$(OR)$_4$}**. The effect is comparable for the two catalysts, as are the changes in the orientation of the "active

ligands" (i.e. hydroxide in S1 and oxyl in S2) and the water molecules interacting with them. While in S1, the methyl group of the bridging acetate ligand connecting Co1 and Co2 is unchanged, in S2, its position is affected by the opening through the rearrangement of the water shell.

We now turn to the states after the water attack has taken place. In S3 and S4, the Co1-O1 distances are similar for **{ErCo$_3$(OR)$_4$}** and **{TmCo$_3$(OR)$_4$}** in both the closed and open cage structures. While the differences in the Ln-OH ligand positions between open and closed cage structures are larger for **{TmCo$_3$(OR)$_4$}** than for **{ErCo$_3$(OR)$_4$}**, the opposite is true for the hmp ligands on Co3 and O3. Their smaller structural change for the opening of **{TmCo$_3$(OR)$_4$}** is associated with the Co1-O3 bond being 0.3 Å smaller in the opened cage structures of **{ErCo$_3$(OR)$_4$}** than in the ones of **{TmCo$_3$(OR)$_4$}** (see above). The largest change in solvation shell structure upon opening of the cubane cage is in S3. The reason for this is that while the OOH ligand in the open cage structures points into the solvation shell and interacts with the water molecules, in the closed ones, it donates a hydrogen bond to the Co1-OH ligand. Due to the steric size and number of possible sites for hydrogen bonding of this ligand, this significantly changes the number and position of water molecules interacting with it and propagates this change far through the solvation shell. The trends in structural differences are not correlated in a simplistic way with the closed-open energy differences since firstly, there are certainly also purely electronic effects at play and secondly, it is of course not trivial in what way a change in orientation of a certain ligand might influence the electronic energy of the catalyst and how this effect might be diminished or enhanced by changes on other ligands. Nevertheless, the observations above underscore once more the necessity of explicitly including solvent molecules in the calculations.

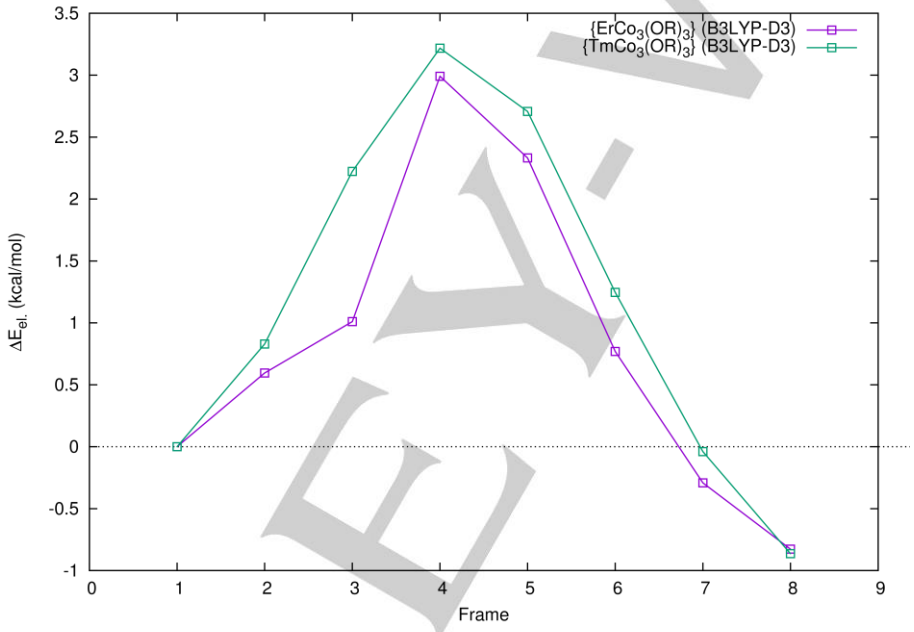

Figure S11. Optimized reaction path for the opening of the catalytic ground state of **{LnCo$_3$(OR)$_4$}** using NEB calculations.

[1] F. H. Hodel, S. Luber, *ACS Catal.* **2016**, *6*, 6750–6761.